

Journal of Materials Chemistry C

Materials for optical, magnetic and electronic devices

Accepted Manuscript

This article can be cited before page numbers have been issued, to do this please use: A. Patelli, G. Seguini, S. Vangelista, S. Spadoni, R. Pezzuto, L. Livellara, F. Milanese, P. Colpani and M. Perego, *J. Mater. Chem. C*, 2026, DOI: 10.1039/D5TC04494D.



This is an Accepted Manuscript, which has been through the Royal Society of Chemistry peer review process and has been accepted for publication.

Accepted Manuscripts are published online shortly after acceptance, before technical editing, formatting and proof reading. Using this free service, authors can make their results available to the community, in citable form, before we publish the edited article. We will replace this Accepted Manuscript with the edited and formatted Advance Article as soon as it is available.

You can find more information about Accepted Manuscripts in the [Information for Authors](#).

Please note that technical editing may introduce minor changes to the text and/or graphics, which may alter content. The journal's standard [Terms & Conditions](#) and the [Ethical guidelines](#) still apply. In no event shall the Royal Society of Chemistry be held responsible for any errors or omissions in this Accepted Manuscript or any consequences arising from the use of any information it contains.

Transport characteristics of 2DHG in p-GaN/AlGaN/GaN heterojunction: impact of Mg dopant activation

Anita Patelli^{1,2}, Gabriele Seguini^{1,*}, Silvia Vangelista³, Simona Spadoni³, Raffaella Pezzuto³,
Luisito Livellara³, Francesca Milanese³, Paolo Colpani³, Michele Perego¹

¹ CNR-IMM, Unit of Agrate Brianza, Via C. Olivetti 2, 20864 Agrate Brianza, Italy

² Università del Piemonte Orientale “A. Avogadro”, Viale T. Michel 11, 15121 Alessandria, Italy

³ STMicroelectronics, Via C. Olivetti 2, 20864, Agrate Brianza, Italy

* Corresponding authors: gabriele.seguini@cnr.it

ABSTRACT

This work investigates the correlation between the two-dimensional hole gas (2DHG) formed at the p-GaN/AlGaN interface and the activation of dopants in the p-GaN layer grown on top of the AlGaN/GaN heterojunction. The effect of annealing environment and temperature on the activation of the Mg impurities within a p-GaN layer is investigated by rapid thermal processing treatments at temperatures ranging from 700 to 900 °C in N₂ and N₂ + O₂ environments. Samples annealed in an N₂ atmosphere exhibited higher sheet resistance (R_s) of $50 \times 10^3 \Omega/\square$ and lower carrier concentration (p) of $1.13 \times 10^{18} \text{ cm}^{-3}$ compared to those annealed in an N₂ + O₂ atmosphere, which had $R_s = 40 \times 10^3 \Omega/\square$ and $p = 1.41 \times 10^{18} \text{ cm}^{-3}$ at room temperature (RT). Sheet resistance and Hall measurement



as a function of temperature were performed on a selected set of samples annealed in N_2+O_2 at 780, 860, and 900 °C to assess effective dopant activation and determine R_s and p values in the p-GaN layer. A pristine sample was used as a reference to monitor possible variation of the R_s and p values upon dopant activation procedure. Analysis of the R_s and p data at $T < 100$ K allowed to distinguish between holes generated from acceptor ionization in the p-GaN layer with an average activation energy 129 ± 4 meV and holes in the 2DHG at the p-GaN/AlGaIn interface with a hole density $\sim 6 \times 10^{12}$ cm⁻². The formation and electrical properties of 2DHG were determined to be completely independent of the activation of Mg impurities in the p-GaN layer.

KEYWORDS: p-GaN/AlGaIn/GaN heterojunction, Mg activation, H concentration, two-dimensional hole gas (2DHG)



INTRODUCTION

View Article Online
DOI: 10.1039/D5TC04494D

Devices based on AlGaN/GaN heterojunctions are used for high-frequency and high-voltage applications in the microelectronics industry, due to the peculiar electrical properties of the two-dimensional electron gas (2DEG) which is naturally formed at the AlGaN/GaN interface^{1,2} without any applied voltage. The creation of this 2DEG results from spontaneous and piezoelectric polarization of the AlGaN layer. A negative voltage supply is necessary to turn off the 2DEG. Normally-on transistors typically require more complex circuit designs. Consequently, significant effort has been concentrated on developing normally-off GaN-based transistors^{3,4}.

Several methods have been recently proposed for fabricating this kind of device. One of the most promising techniques is the formation of a deep gate recess by the local removal of AlGaN layer, resulting in localized depletion at the AlGaN/GaN interface⁴⁻⁷. Another widely investigated approach is based on the epitaxial growth of a p-type gate material, such as p-GaN, on top of the AlGaN film to shift the conduction band upwards, thus depleting the channel even at zero applied gate voltage^{8,9}.

Both these approaches have advantages and limitations. Using a gate recess with a gate insulator leads to a very low gate leakage current and fine control of the threshold voltage but can favor trapping at the interfaces and/or in the insulator. Moreover, fine-tuning of the etching process is necessary to prevent mobility degradation at the AlGaN/GaN interface. Conversely, using a p-type gate material requires fine control of the doping process and activation of the Mg impurities that are used as p-type dopants. The introduction of an additional growth step increases the complexity of the fabrication process, but this approach guarantees lower on-resistance and high mobility¹⁰. In this respect, p-GaN integration represents a cost-effective solution for the fabrication of enhancement mode FET devices.

Interestingly, several studies¹¹⁻¹³ demonstrated the formation of a two-dimensional hole gas (2DHG) at the p-GaN/AlGaN interface, stimulating an intense research activity aiming at the fabrication of p-FET devices for the development of GaN based CMOS logic circuits. *Ng et al.*¹³



claim that the 2DHG originates from the ionization of Mg acceptors in the AlGaN barrier. However, a weak temperature-dependent concentration of holes in the 2DHG is observed by variable temperature Hall effect measurements, suggesting that the mechanism inducing the formation of the 2DHG is somehow independent of the ionization of Mg impurities. In a very recent paper, Kumar *et al.*¹⁴ indicate that precise control over doping, material thickness, and composition is essential for optimizing pFET performance and reliability for next-generation electronic applications on GaN. Nevertheless, the effective correlation between doping of p-GaN and formation of the 2DHG has not been completely clarified.

This work focuses on optimizing the activation of Mg dopants in a p-GaN film epitaxially grown on top of an AlGaN/GaN heterojunction and correlating it with the electrical properties of the 2DHG that is formed at the p-GaN/AlGaN interface. The objective is to gain a deeper comprehension of the intricate relationship between the processing conditions necessary for Mg activation and the formation of the 2DHG. A comprehensive understanding of how processing conditions influence the characteristics of both the 2DHG and the 2DEG is paramount for the effective utilization of the 2DHG as a fundamental building block in the fabrication of p-channel devices on the GaN substrate taking advantage of a technologically relevant platform that could facilitate future exploitation. Mg dopants were introduced into the p-GaN during the growth process. The Mg impurities activation was achieved through high-temperature thermal treatment ($T > 600$ °C) using a rapid thermal processing (RTP) system in N_2 and $N_2 + O_2$ environments^{15,16–19}. Transport measurements as a function of temperature were performed on selected samples to discriminate between the holes in the 2DHG and those in the p-GaN layer, providing information about hole density and mobility in the 2DHG as a function of the Mg impurity activation in the p-GaN layer. Upon selective removal of the p-GaN, low temperature characterization of the 2DEG at the AlGaN/GaN buried interface was performed, enabling a direct comparison between the properties of the 2DHG and 2DEG that are formed at the



different interfaces of the p-GaN/AlGa_xN/GaN stack.

View Article Online
DOI: 10.1039/D5TC04494D

EXPERIMENTAL METHODS

A commercial 200 mm GaN-on-Si wafer was used for this study. It comprises a ~ 100 nm thick p-GaN layer with a nominal Mg doping concentration of $2 \times 10^{19} \text{ cm}^{-3}$. The p-GaN layer was grown by Metal-Organic Chemical Vapor Deposition (MOCVD) on top of a stack consisting of a thick ~ 18 nm Al_xGa_{1-x}N barrier layer with 20% of Al content and a GaN buffer layer. A scheme of interface atomic composition, sample structure and band structure of the heterojunction is reported in **Figures 1a, 1b** and **1c**, respectively. Samples measuring $1 \times 1 \text{ cm}^2$ were cut out from the wafer. These samples underwent thermal treatments in an RTP machine (AS-One150 RTP system) at temperatures ranging from 700 to 900 °C in N₂ and N₂ + O₂ (5%) atmospheres. A non-annealed $1 \times 1 \text{ cm}^2$ sample was used as a reference to assess the effective activation of Mg dopant impurities upon annealing. In the following, this sample is referred to as the pristine sample.

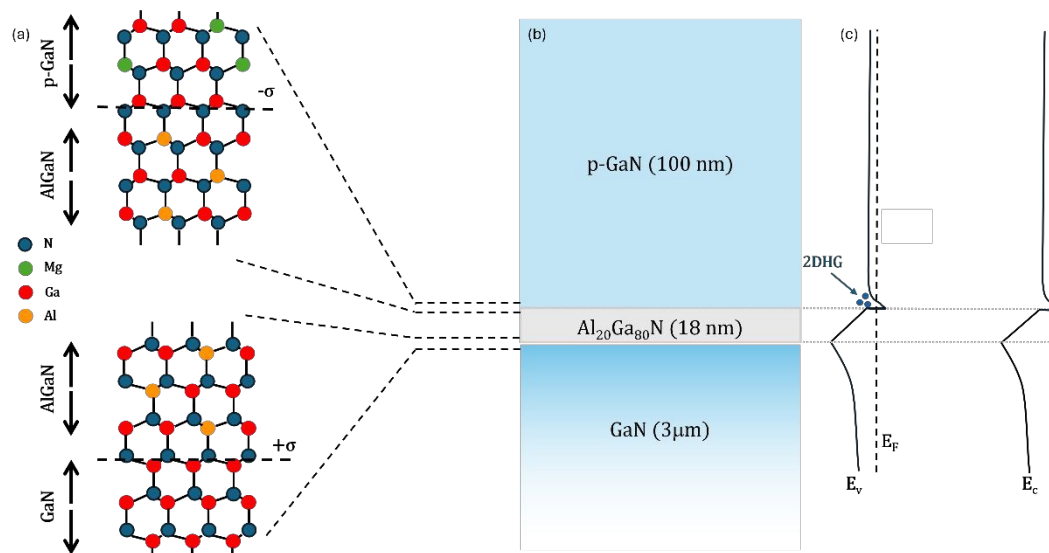


Figure 1: Atomic structure (a), cross section (b) and band diagram (c) of p-GaN/AlGa_xN/GaN heterojunction

Chemical information about the dopant and impurity distributions in the samples was obtained using Time-of-Flight Secondary Ion Mass Spectrometry (ToF-SIMS) with an ION-TOF M6 system. The base pressure in the main chamber was kept at 1×10^{-10} mbar to prevent moisture physisorption on the sample surface and minimize the H background signal. All the measurements were performed



in interlaced mode, operating in positive or negative mode for Mg and H detection, respectively.

For the electrical characterization of the p-GaN/AlGaIn interface, p-type Ohmic contacts were fabricated by depositing Pd/Au (80/20 nm) metal stacks at the corners of each $1 \times 1 \text{ cm}^2$ sample, whereas for the electrical characterization of the AlGaIn/GaN interface, upon selective removal of p-GaN layer, Ti/Al/Ni/Au (15/80/20/80 nm) metal stacks were deposited at the corners of each $1 \times 1 \text{ cm}^2$ sample and annealed with rapid thermal treatment at $800 \text{ }^\circ\text{C}$ for 300 s forming n-type Ohmic contacts on AlGaIn/GaN heterostructure²⁰. Sheet resistance (R_s) and Hall effect measurements in Van der Pauw configuration were performed at temperatures ranging from 5 to 300 K with a magnetic field varying from -0.8 to 0.8 T by means of a Bruker BE15 magnet and a He-based cryogenic system. In addition, a homemade system with a Eurotherm heater controller was used for R_s measurements in the range of temperatures between 300 and 600 K. The Hall factor is unity, and the calculated field effect mobility can be compared directly with the Hall-effect mobility.

RESULTS AND DISCUSSION

Figure 2a reports R_s values at room temperature (RT) as a function of annealing temperature for the two different annealing environments: N_2 (orange squares) and $\text{N}_2 + \text{O}_2$ (green circles). The dashed blue line indicates the sheet resistance ($R_s = 52 \text{ k}\Omega/\square$) of the pristine sample which serves as a reference. Accordingly, resistivity in pristine sample is determined to be $\rho = 0.52 \text{ }\Omega \text{ cm}$, significantly lower than the values ($\rho > 10 \text{ }\Omega \text{ cm}$) reported for undoped GaN films^{21,22}. Although the resistivity in undoped GaN films depends on growth and processing conditions²¹, the measured resistivity value suggests that, even without thermal treatment, a fraction of Mg impurities in the pristine sample has already been activated during growth. The annealed samples exhibit lower R_s values compared to the pristine sample. For the samples annealed in the N_2 atmosphere, R_s decreases as the annealing temperature increases, from $48 \pm 2 \text{ k}\Omega/\square$ at $700 \text{ }^\circ\text{C}$ to $34 \pm 1 \text{ k}\Omega/\square$ at $900 \text{ }^\circ\text{C}$. Conversely, samples annealed in the $\text{N}_2 + \text{O}_2$ atmosphere exhibit a less pronounced decrease in R_s as the annealing



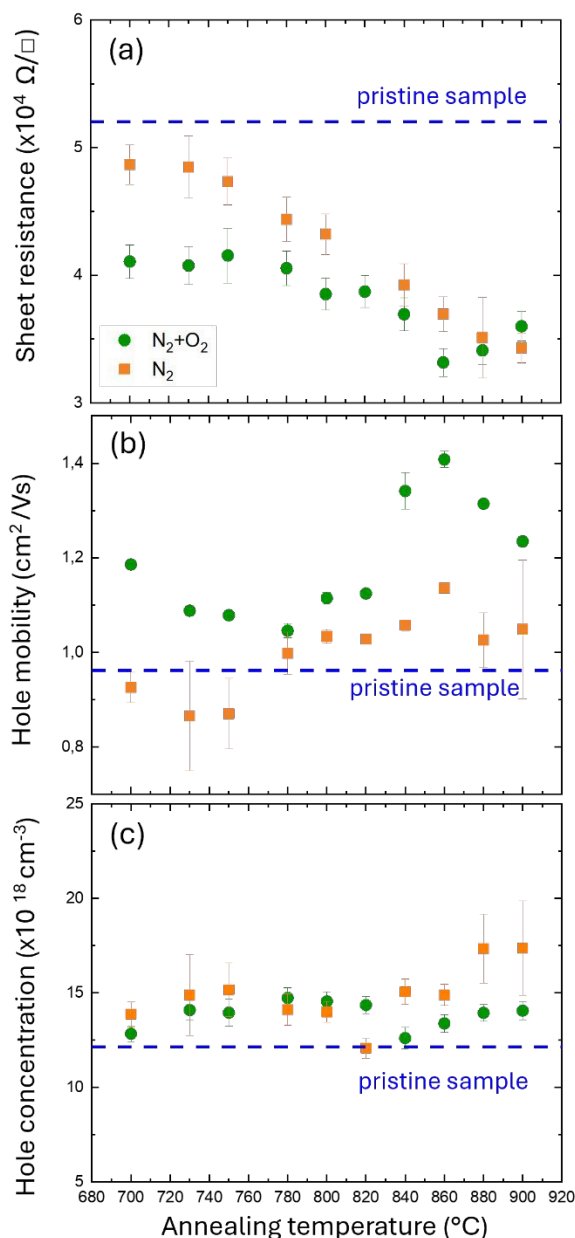


Figure 2: Sheet resistance (a), carrier concentration (b), and mobility (c) at room temperature as a function of annealing temperature for two different annealing atmospheres: N_2 (orange squares) and $N_2 + O_2$ (green circles). The dashed blue lines represent the sheet resistance (a), carrier concentration (b) and mobility (c) values for the pristine sample.

temperature rises. R_s is at its lowest value at 860 °C ($33 \pm 1 \text{ k}\Omega/\square$). Further increasing the annealing temperature causes a slight rise of R_s up to $36 \pm 1 \text{ k}\Omega/\square$ at 900 °C. Comparing the results for the two annealing atmospheres, it is quite evident that, at temperatures below 860 °C, samples annealed in N_2 exhibit higher R_s values than those annealed in $N_2 + O_2$. This result is perfectly consistent with data reported by Kumar *et al.*¹⁷, which indicates that oxygen promotes the dissociation of Mg-H



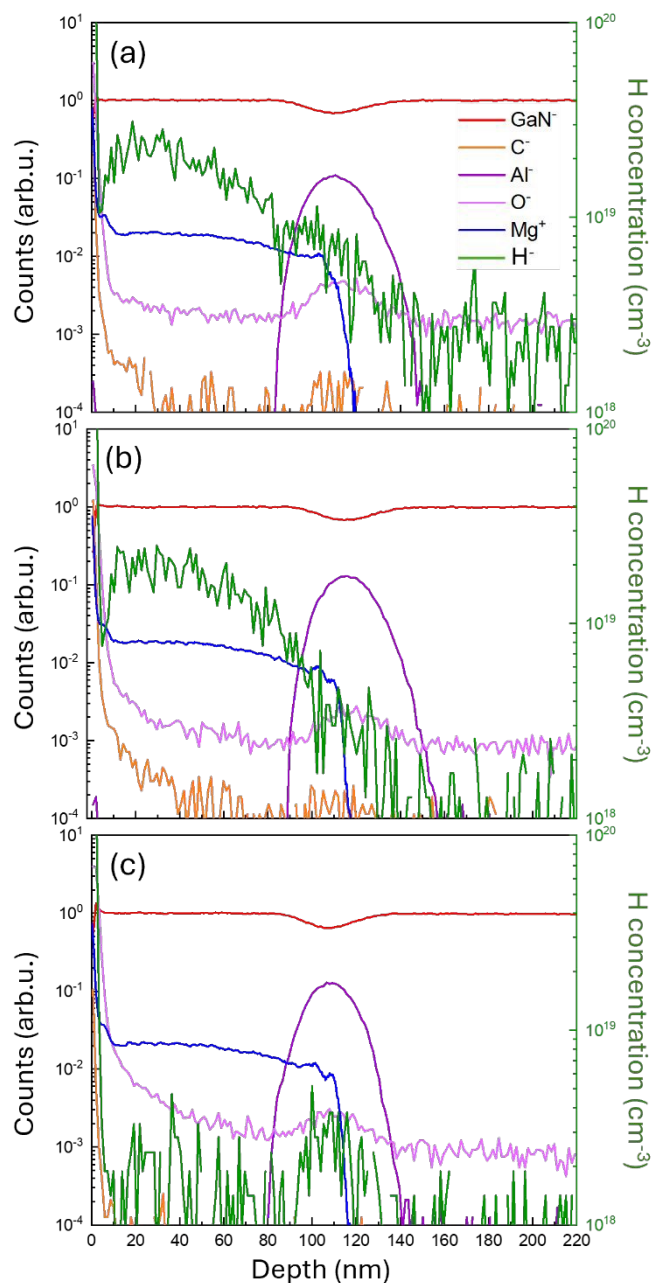


Figure 3: (a) H dose of p-GaN layer as a function of annealing temperature for two different atmosphere conditions N_2 (orange squares) and $N_2 + O_2$ (green circles). The dashed blue line represents the H dose of the pristine sample. (b) H dose as a function of sheet resistance for two different annealing atmospheres N_2 (orange squares) and $N_2 + O_2$ (green circles). In blue, the value for the pristine sample. In the inset, oxygen ToF-SIMS depth profile for each annealing temperature in $N_2 + O_2$ atmosphere.

complexes. **Figure 2b** shows the hole concentration (p) values as a function of annealing temperature, obtained through Hall effect measurements at RT. The pristine sample exhibits a p of $9.6 \pm 0.6 \times 10^{17} \text{ cm}^{-3}$, which is comparable to that of the samples annealed in N_2 atmosphere (orange squares). Samples annealed in the $N_2 + O_2$ atmosphere (green circles) exhibit a higher p than those annealed in N_2 .



Moreover, data in **figure 2b** indicate that for the samples annealed in N_2 , p does not vary significantly over the range of annealing temperatures considered, within the experimental error. On the other hand, in the samples annealed in $N_2 + O_2$, p progressively increases with an increasing annealing temperature from 760 to 860 °C, reaching a maximum value of $1.41 \pm 0.02 \times 10^{18} \text{ cm}^{-3}$ at 860 °C before decreasing at higher temperatures. Carrier mobility (μ) is computed by combining R_s and Hall measurements according to equation $\mu = (1/q p R_s)$. μ values of the different samples are reported in **Figure 2c**. Interestingly, μ does not show significant variation from sample to sample, irrespective of the different annealing atmospheres. The pristine sample shows a slightly lower μ (blue dashed line)

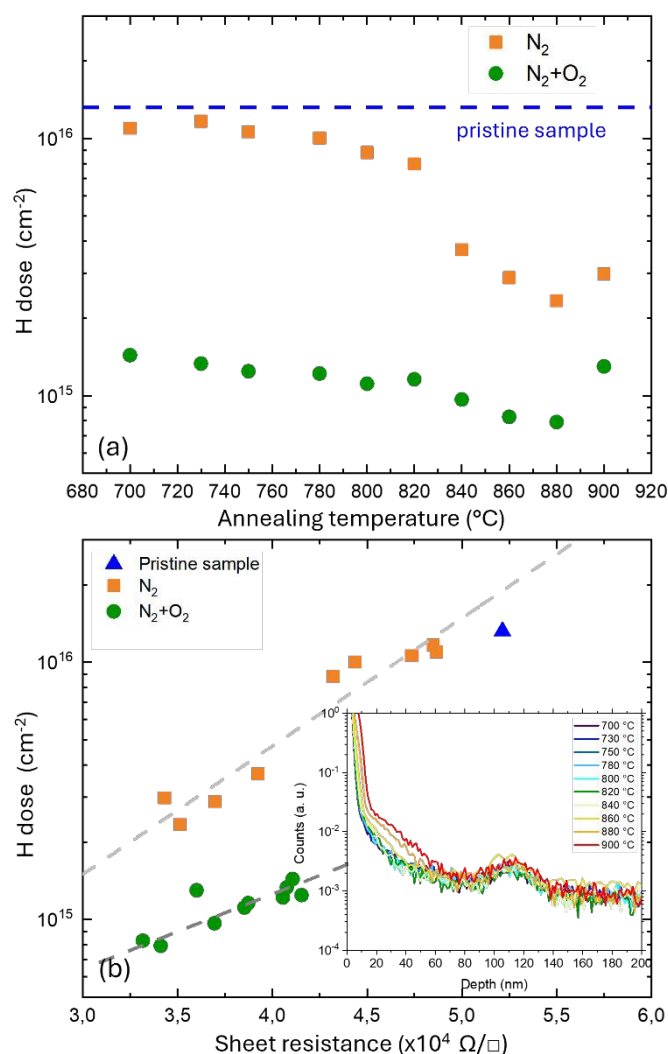
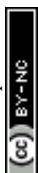


Figure 4: ToF-SIMS depth profiles showing Mg (blue line) and calibrated H depth profile (green line, right axis scale) for pristine sample (a), samples annealed at 780 °C in N_2 (b) and in $N_2 + O_2$ (c). GaN^- and Al^- secondary ion signals are reported without any calibration to simply indicate the position of the different interfaces in the $p\text{-GaN}/\text{AlGaN}/\text{GaN}$ heterojunction



value than the annealed ones. Moreover, for samples annealed in $N_2 + O_2$ atmosphere μ appears to be temperature independent. On the other hand, for samples annealed in N_2 , μ show a small trend as a function of temperature; μ increases as the temperature increases.

Figure 3 reports representative ToF-SIMS depth profiles of the pristine sample **(a)** and of the samples annealed at 780 °C in N_2 **(b)** and $N_2 + O_2$ **(c)**. The different secondary ion signals were normalized to the average GaN^- signal value in the p-GaN layer to account for primary ion current variation during the measurements. The Al^- signal (purple line) is reported to visualize the AlGaN layer. In correspondence with the AlGaN layer, a decrease of GaN^- signal intensity (red line) is observed. The Mg^+ signal (blue line) is uniform in the p-GaN layer and decreases quite sharply in the AlGaN layer. It is interesting to note that the Mg^+ signal does not change across the different samples, indicating that the Mg distribution was not affected by the thermal treatment resulting in no significant diffusion of Mg impurities in the AlGaN layer. The orange line corresponds to the C^- signal and represents the carbon depth distribution. The intense C^- signal at the surface of the sample is essentially related to carbon contamination due to air exposure. The tails of the C^- signals in the pristine sample and in the samples annealed in N_2 atmosphere are quite similar, suggesting a similar level of carbon contamination in the p-GaN layer. Conversely, carbon contamination is reduced in samples annealed in the $N_2 + O_2$ atmosphere. It is worth noting that C impurities are reported to increase GaN resistivity^{23–25}. An intense O^- background signal is present in all samples, due to the contamination during depth profiling by the residual oxygen and moisture in the analysis chamber. However, in the sample annealed in $N_2 + O_2$ atmosphere, the intensity of the O^- signal in the p-GaN layer is higher than in the pristine sample and in the one annealed in N_2 atmosphere; this could be caused by the diffusion of oxygen into the p-GaN during the annealing process. The green line represents the calibrated H depth profile (right axis scale). Data indicates only a slight difference between the pristine sample and the samples annealed in N_2 . Conversely, the H profile in the sample annealed in $N_2 + O_2$ atmosphere is considerably lower than in the other samples, consistently with



previous results by *Kumar et al.*¹⁷.

View Article Online
DOI: 10.1039/D5TC04494D

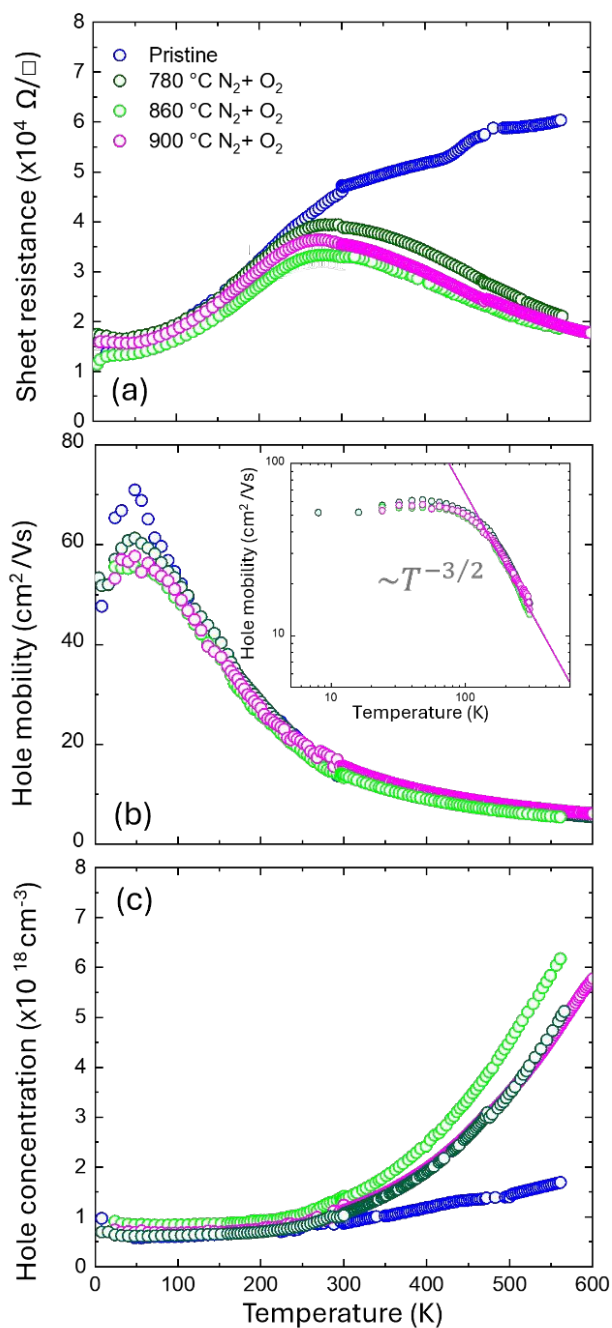


Figure 5: (a) Measured sheet resistance values as a function of the temperature for pristine sample (blue circles) and annealed in $N_2 + O_2$ at 780 (dark green circles), 860 (light green circles) and 900 °C (magenta circles). Carrier mobility (b) and carrier concentration (c) as a function of the temperature for pristine (blue circles) and samples annealed in $N_2 + O_2$ at 780 °C (dark green circles) and 860 °C (light green circles). Mobility and carrier concentration are measured in the range of temperature between 5-300 K by Hall effect measurement. The carrier mobility values for temperature in the range of 300-600 K are obtained by fitting the mobility as a $T^{-3/2}$ function, as shown in the inset of panel (b). Hole concentration values have been calculated using sheet resistance data and mobility values.

By integrating the H concentration profile in the p-GaN region, the total H dose in the p-GaN layer for each sample was determined. **Figure 4a** shows the total H dose as a function of annealing



temperature for the two different annealing atmospheres. For annealing temperatures $T < 780^\circ\text{C}$, the H dose in the samples annealed in N_2 is quite close to that of the pristine sample (dashed blue line). The H dose then decreases slightly as the annealing temperature rises to 820°C . The reduction of the H dose becomes more pronounced at temperatures $T > 820^\circ\text{C}$. Samples annealed in $\text{N}_2 + \text{O}_2$ exhibit almost temperature-independent behavior with a significant reduction in H dose upon annealing, even at low temperatures. Interestingly, irrespective of the annealing atmosphere, a small increase in the H dose is observed in the samples annealed at 900°C . These data clearly highlight that, for each annealing temperature, the samples annealed in N_2 have a higher H dose than those annealed in $\text{N}_2 + \text{O}_2$. As reported in literature ²⁶, O_2 promotes the dissociation of Mg-H complexes during thermal treatment, increasing Mg activation, and reducing R_s of the p-GaN layer.

Figure 4b shows the H dose as a function of R_s for the samples annealed in N_2 and in $\text{N}_2 + \text{O}_2$. The blue triangle corresponds to the pristine sample. In the annealed samples, the reduction in R_s is systematically associated with a decrease in the H dose, irrespective of the annealing atmosphere. Despite the similar trend, it is noteworthy that samples with the same resistivity are characterized by different H content depending on the annealing atmosphere. This difference suggests that the varying activation levels of Mg impurities in the two sets of samples cannot be fully explained only by differences in H concentration. An additional contribution should be considered, that is oxygen diffusion into the p-GaN layer during the annealing process. This is particularly evident in samples annealed in $\text{N}_2 + \text{O}_2$ atmosphere. Oxygen depth profiles for samples annealed in $\text{N}_2 + \text{O}_2$ are reported in the inset of **figure 4b**. The tails of the O^- signal indicate that, at the highest annealing temperatures, the oxygen diffusion into the p-GaN layer near the surface is significant. Oxygen is an n-type dopant impurity for GaN, and the increased oxygen content could lead to charge compensation, reducing the availability of holes in the GaN layer. Carbon residues may play an additional role. Carbon impurity may preferentially form deep level traps, acting as effective compensation centers and leading to an increase in resistivity ²⁴. This behavior of R_s as a function of the annealing conditions is not yet fully



understood, and further experiments are necessary to fully elucidate this point.

View Article Online
DOI: 10.1039/D5TC04494D

At RT, R_s values exhibit a relatively small variation from sample to sample. To gain a deeper understanding of the differences in terms of activation, R_s measurements were performed at temperatures ranging from 5 to 600 K for four different samples: one pristine sample (blue symbols) and three samples annealed in $N_2 + O_2$ at 780 (dark green symbols), 860 (light green symbols) and 900 °C (magenta symbols), respectively. R_s values as a function of the temperature for these samples are reported in **figure 5a**. All the samples behave in a quite similar manner at temperatures below RT ($T < 300$ K): R_s decreases as the temperature decreases, likely due to the progressive reduction of acoustic phonon scattering. Interestingly, this behavior differs from what we would expect for a

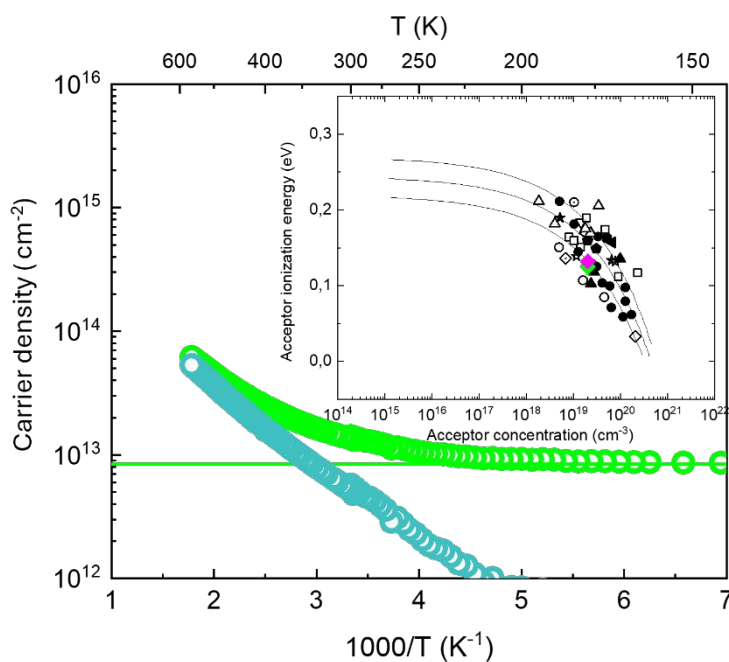


Figure 6: Hole density (light green symbol) as a function of temperature for sample annealed at 860 °C in $N_2 + O_2$. The values at low temperature had been fitted (light green line) to obtain 2DHG contribution. This contribution has been removed to have just Mg impurities after subtracting of 2DHG hole density (dark green line). In the inset, comparison between our results (dark green 780 °C, light green 860 °C and magenta 900 °C) and literature data from ● Brochen et al., ◇ Namkoong et al., ★ Leroux et al., ▽ Konczewicz et al., ◁ Nakayama et al., ◀ Tanaka et al., ▢ Nguyen et al., ◆ Kim et al., ◇ Huang et al., ☆ Nikishin et al., ⊙ Nakano et al., □ Kozodoy et al., ○ Ke et al., △ Gotz et al.. The solid lines represent simulations for different ionization energy values according to equation $E_a = E_{a0} - \alpha N_A^{1/3}$ where $\alpha = \Gamma(2/3) \cdot (4\pi/3)^{1/3} (q^2/4\pi\epsilon)$ ²⁷

semiconductor, where a progressive increase of R_s is typically observed due to thermal deionization of Mg impurities. Conversely, above RT ($T > 300$ K), the pristine and annealed samples exhibit



notably different R_s evolutions. For the annealed samples, R_s decreases with increasing temperature while for the pristine samples, R_s increases with increasing temperature. This differing evolution of R_s as a function of temperature can be explained by assuming that, in the pristine sample, only a small fraction of the impurities is electrically activated.

Consequently, the resistivity increases because the carrier mobility is reduced by increasing phonon scattering. Conversely, for the annealed samples, as the temperature increases, the fraction of ionized impurities progressively grows, resulting in a decrease in R_s . Hall measurements were performed over the temperature range of 5 to 300 K. Experimental values of carrier mobility and concentration are reported in **figure 5b** and **5c**, respectively. Within this temperature range, μ progressively increases as the temperature decreases to approximately 80 K. However, at higher temperatures, a clear reduction in μ is observed (**Figure 5b**). This temperature-dependent evolution is consistent for both pristine and annealed samples. μ for $T > 300$ K were extrapolated by fitting the μ in the temperature range from 200 to 300 K with a $T^{-3/2}$ function, as shown in the inset of **figure 5b**. This extrapolation assumes that, in this specific temperature range, carrier mobility evolution is primarily determined by acoustic phonon scattering, consistent with data reported in literature¹³. The extrapolated μ for $T > 300$ K, along with the measured μ for $T \leq 300$ K, are reported in **figure 5b**.

Figure 5c reports measured p values as a function of temperature for $T < 300$ K. At temperatures above RT, p were calculated by combining R_s data and extrapolated μ values. In this range of temperatures ($T > 300$ K), the estimated p are found to increase with temperature for all samples. This supports the idea that raising the temperature causes the ionization of Mg impurities that are not fully ionized at RT. Interestingly, p of annealed samples increase with the temperature at steeper slopes compared to the pristine samples. However, temperatures below RT, all the samples exhibit the same behavior: p progressively decreases and then levels off, reaching a plateau at $T > 200$ K. The persistence of a significant number of carriers at very low temperatures indicates a metallic-like



behavior which is associated to the formation of a 2DHG at the p-GaN/AlGaIn/ interface¹³ View Article Online
DOI: 10.1039/D5TC04494D

Since at $T < 100$ K all the Mg impurities are thermally frozen, we estimated the 2DHG contribution to the hole density as the average value of the total hole density in the temperature range between 20 and 100 K. This contribution was subtracted from the total hole density to highlight the contribution of the holes generated by thermal ionization of Mg impurities. **Figure 6** shows the total hole density (light green symbols) and the calculated bulk hole density (light blue symbols). The calculated bulk hole density decreases with decreasing temperature, which is consistent with the thermal deactivation of Mg impurities. Analyzing the different contributions as a function of temperature, we can observe that at low temperatures the only contribution present is from the 2DHG. At RT, both contributions are equally relevant, whereas at temperatures above RT, ionization of Mg impurities progressively increases, increasing the relevance of this bulk contribution to conduction. In addition, by fitting the extrapolated bulk hole density by an exponential function the activation energy (E_A) of Mg impurities ($\approx E_A/kT$) was estimated to be (125 ± 11) meV.

| Annealing temperature [°C] | p (300 K) [cm ⁻²] | P _{2DHG} [cm ⁻²] | E _a [meV] | Mobility (300 K) [cm ² /Vs] | Mobility (80K) [cm ² /Vs] |
|----------------------------|-------------------------------|---------------------------------------|----------------------|--|--------------------------------------|
| 0 | 1,0×10 ¹³ | 0,6×10 ¹³ | 70 | 15 | 60 |
| 780 | 1,0×10 ¹³ | 0,6×10 ¹³ | 126±8 | 17 | 56 |
| 860 | 1,4×10 ¹³ | 0,8×10 ¹³ | 125±11 | 14 | 53 |
| 900 | 1,2×10 ¹³ | 0,7×10 ¹³ | 132±6 | 15 | 54 |

Table 1: Calculated and measured values for the samples considered pristine and annealed at 780, 860, and 900 °C in N₂ + O₂.

This procedure was repeated for the pristine sample and the other two samples annealed in N₂ + O₂ at 780 and 900 °C, respectively. The results of this analysis are summarized in **Table 1** that reports total hole concentration, hole concentration in the 2DHG, as well as activation energy and hole mobility at RT and at low temperature ($T = 80$ K). Interestingly the activation energy of the Mg impurities in the p-GaN layer was found to be roughly the same for all the samples. The calculated values are reported in the inset of figure 5 together with data collected from the literature at different Mg concentrations²⁸. The calculated E_a values are in excellent agreement with those reported in the



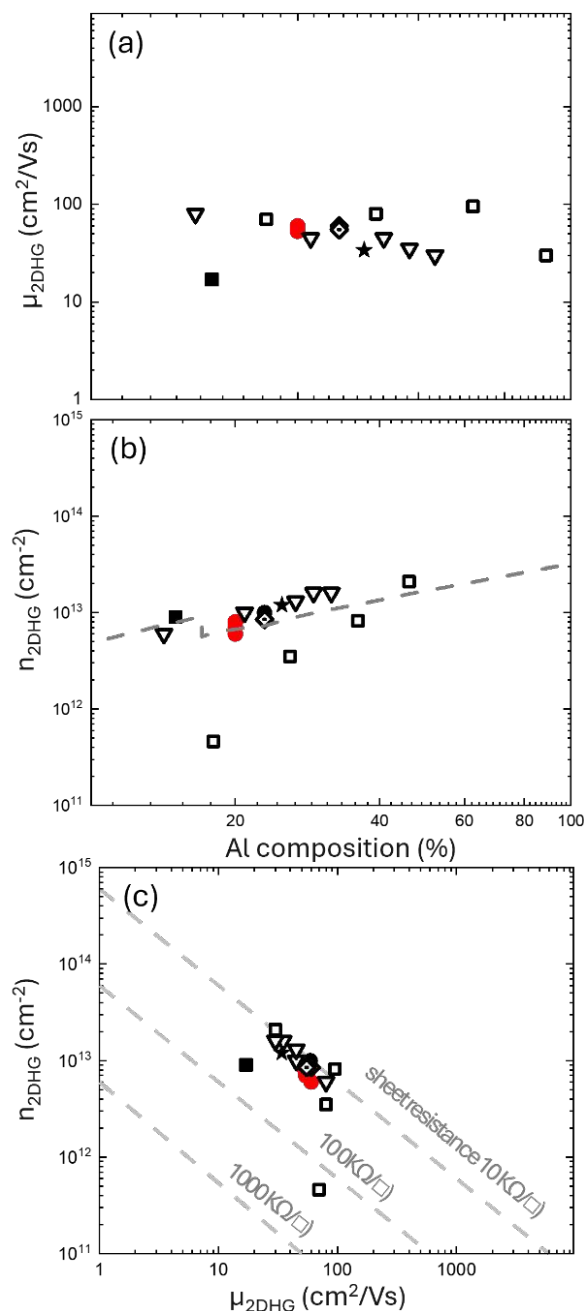


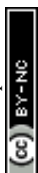
Figure 7: Comparison of our data (red solid circles) and the literature data from ● Nakajima et al.²⁹, ★ Ng et al.¹³, ▽ Beckmann et al.³⁰ □ Shao et al.¹², □ Zhang et al.³⁴, ◇ Nakajima et al.³¹. Figures (a) and (b) show the 2DHG hole density and hole mobility, respectively, measured at $T < 100$ K as a function of the Al content (%) in the AlGaN layer. The dotted grey line in panel (b) indicate theoretical hole density as function of the hole concentration calculated taking into account strain relaxation³³. (c) hole density as a function of hole mobility in the 2DHG.

literature for a Mg concentration around $1 \times 10^{19} \text{ cm}^{-3}$ ²⁸. This result further supports the idea that, at $T = 80$ K, no holes generated by thermal ionization of Mg impurities are present in the p-GaN and that the conduction is essentially dominated by the holes in the 2DHG at the p-GaN/AlGaN interface.



Interestingly, the carrier concentration and mobility values measured at this low temperature do not significantly change upon Mg activation. In particular, hole mobility and hole concentration at $T = 80$ K are quite similar to those obtained in the annealed samples at low temperatures, suggesting that the characteristics of 2DHG are essentially independent of the activation process.

In **Figure 7** the hole concentration and hole mobility at $T = 80$ K are compared with those reported in literature for 2DHG formed at p-GaN/AlGaIn heterojunctions with Al content ranging from 15 to 50%^{11–13,27–30}. **Figure 7a** shows that the mobility is almost independent from Al content in the AlGaIn layer with values that are always below $100 \text{ cm}^2/\text{Vs}$. Conversely, as shown in **Figure 7b**, hole density exhibits a weak correlation with Al composition, with p value slightly increasing as the Al content in the AlGaIn layer increases. Finally, 2DHG mobility as a function of hole density is shown in **Figure 7c**. Gray dashed lines indicate sheet resistance isolines, highlighting an upper limit for the sheet resistance in this system, because of a progressive reduction of mobility when increasing carrier density in the 2DHG layer. In view of a possible exploitation of 2DHG formed at p-GaN/AlGaIn interface in p-FET device, it is worth to compare the carrier density and mobility of the 2DHG with those of the 2DEG that is formed at the buried AlGaIn/GaN interface. To achieve this goal, R_s , carrier density, and mobility of the 2DEG as a function of temperature have been measured on the same substrate after the removal of the p-GaN layer by chemical etching. **Figure 8** presents a direct comparison of the electrical characteristics of the 2DEG and 2DHG at the AlGaIn/GaN and p-GaN/AlGaIn interfaces for the sample annealed at 860°C in $\text{N}_2 + \text{O}_2$. **Figure 8a** clearly demonstrates that the 2DHG exhibits a considerably higher R_s compared to 2DEG. In addition, the 2DEG shows the typical increase in R_s with increasing temperature, determined by the mobility reduction due to phonon scattering. The mobility evolution as function of temperature for the 2DHG at the p-GaN/AlGaIn interface is very different because of the progressive ionization of Mg impurities leading to a R_s plateau value at RT. Mobility values as a function of temperature are reported in **Figure 8b** emphasizing a significant difference in the absolute values between the 2DHG and 2DEG,



respectively. This difference is due not only to the higher effective mass of holes, but also to the distinct effects of polar optical and acoustic phonons, which result in higher mobility³². *Poncé et al.* investigated the atomic-scale mechanisms responsible for the low hole mobility in GaN. They showed that the origin of the low hole mobility lies in carrier scattering within the light-hole (LH) and heavy-hole (HH) bands. The high density of states associated with the LH and HH bands plays a central role in reducing hole lifetimes and, consequently, suppressing their mobility. Additional factors further contributing to the reduced hole mobility are the presence of multiple scattering channels and the strong non-parabolicity of the HH band. However, their study was limited to bulk GaN and did not directly investigate hole mobility in heterojunctions³³. Conversely, in their work, *Bader et al.*³² proposed a specific model to explain the limited hole mobility of the 2DHG at the GaN/AlN interface. More precisely, they determined the spectra of both acoustic and optical phonons in the heterostructure and proposed that the mobility limitations are associated to phonon scattering at the GaN/AlN interface. Nevertheless, this mechanism remains an active area of investigation. Interestingly, according to our experimental data, hole and electron mobilities exhibit the same temperature dependence suggesting that the same mechanisms govern the evolution of mobility as a function of temperature for both systems: namely, defects and interface roughness at low temperatures, and phonon scattering at high temperatures. **Figure 8c** shows that the carrier density is significantly higher in the case of 2DHG. As RT approaches, hole density exhibits a different temperature dependence due to the progressive ionization of Mg impurities. These results demonstrate that the significantly higher sheet resistance of the 2DHG is essentially ascribed to the limited hole mobility. The limited hole mobility in the 2DHG represents a fundamental limitation for the implementation of complementary FET technology on this specific technological platform exploiting p-FET devices taking advantage of a 2DHG as a transistor channel. A comparison with Si CMOS technology is instructive, as it remains highly successful despite the difference in mobility between electrons and holes. In silicon, at room temperature, electrons move approximately three times faster than holes due to their lower effective mass compared with holes. However, this

View Article Online
DOI: 10.1039/D5TC04494D



difference can be compensated through appropriate device design. In contrast, in GaN-based heterostructures the mobility of electrons in the 2DEG is typically two orders of magnitude higher than that of holes in the 2DHG. Such a large disparity cannot be easily compensated by simply adjusting the device design at the circuit level¹⁴. Accordingly, several studies investigated alternative strategies to circumvent this specific problem, considering different materials such as AlN to reach higher mobilities and higher carrier densities at the GaN/AlN interface. *Zhang et al.*³⁴ reported mobility value of 280 cm²/Vs at 10K, in GaN/AlN heterostructures. As previously discussed, *Bader et al.*³² presented an intriguing approach to enhance hole mobility in GaN/AlN heterostructures grown on sapphire substrates. While their findings are noteworthy, the integration of GaN/AlN heterostructures onto a GaN platform presents significant challenges, hindering the direct application of their scientific outcomes. Very recently an alternative approach has been proposed to address this problem by adjusting structural parameters of the p-GaN/AlGaIn/GaN double heterojunction to fabricate p-FET with performance and reliability characteristics that could be suitable for next-generation electronic applications¹⁴.

CONCLUSION

The activation of Mg impurities inside a GaN layer was investigated as a function of different annealing conditions. The annealing atmosphere and temperature significantly affect the R_s and the carrier transport characteristics. In detail, annealing in a N₂ + O₂ atmosphere guarantees lower R_s and higher p than annealing in N₂. Carrier mobility has similar values for all the samples considered, irrespective of the annealing conditions. ToF-SIMS analysis shows a reduction in H concentration upon annealing. The trend of the H dose in each atmosphere as a function of R_s shows that the presence of hydrogen has a negative impact on the material's resistance, according to the correlation between the H dose in the p-GaN layer and R_s data. Hall and R_s measurements as a function of temperature highlighted the differences between annealed samples and pristine sample pointing out the different levels of activation of the Mg impurities. The mean value for approximately samples of



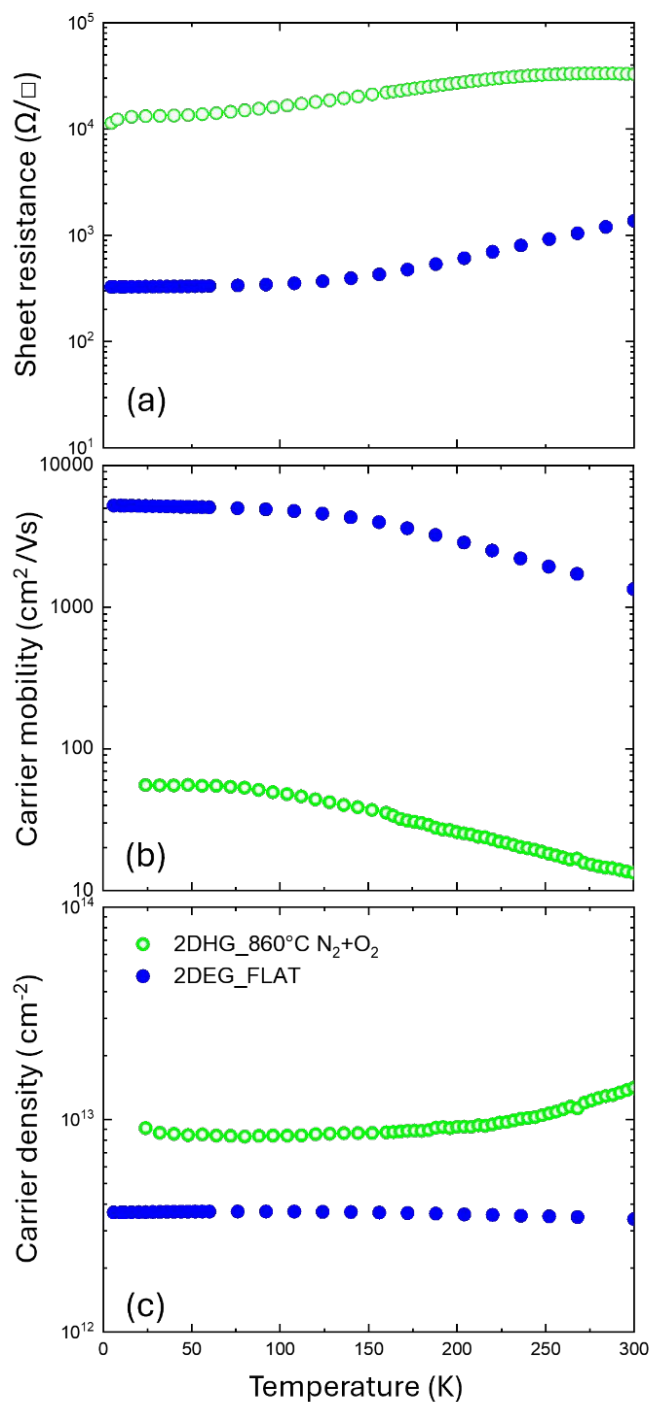


Figure 8: Comparison of sheet resistance (a), hole mobility (b), and hole density (c) for 2DEG (blue symbols) and 2DHG (green symbols) of annealed sample at 860 °C in $N_2 + O_2$.

the Mg activation energy was determined to be $E_A = (129 \pm 4)$ meV. At temperatures below 100 K, the hole concentration is found to be constant providing a clear signature of the presence of 2DHG at the interface between the p-GaN and AlGaN layers. This result is perfectly consistent with other reports in the literature and introduces important constraints in the design of the GaN based heterostructures devices to be carefully evaluated. On the other hand, even if hole mobility in the



2DHG is quite limited compared with the one of 2DEG, the presence of this conductive channel at the p-GaN/AlGa_N interface opens to an interesting scenario with the possibility to fabricate p-type transistor on GaN paving the way to CMOS technology implementation. To further explore this application, it is necessary to improve the mobility of the 2DHG by proper engineering of the heterostructure.

Conflicts of interest

There are no conflicts to declare.

Data availability

The data supporting this article have been included as part of the Supplementary Information.



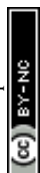
References

View Article Online
DOI: 10.1039/D5TC04494D

1. Ishida, M., Ueda, T., Tanaka, T. & Ueda, D. GaN on Si Technologies for Power Switching Devices. *IEEE Trans. Electron Devices* **60**, 3053–3059 (2013).
2. Meneghini, M. *et al.* GaN-based power devices: Physics, reliability, and perspectives. *Journal of Applied Physics* **130**, 181101 (2021).
3. Cai, Y., Zhou, Y., Lau, K. M. & Chen, K. J. Control of Threshold Voltage of AlGaIn/GaN HEMTs by Fluoride-Based Plasma Treatment: From Depletion Mode to Enhancement Mode. *IEEE Trans. Electron Devices* **53**, 2207–2215 (2006).
4. Lanford, W. B., Tanaka, T., Otoki, Y. & Adesida, I. Recessed-gate enhancement-mode GaN HEMT with high threshold voltage. *Electron. Lett.* **41**, 449–450 (2005).
5. Oka, T. & Nozawa, T. AlGaIn/GaN Recessed MIS-Gate HFET With High-Threshold-Voltage Normally-Off Operation for Power Electronics Applications. *IEEE Electron Device Lett.* **29**, 668–670 (2008).
6. Saito, W., Takada, Y., Kuraguchi, M., Tsuda, K. & Omura, I. Recessed-gate structure approach toward normally off high-Voltage AlGaIn/GaN HEMT for power electronics applications. *IEEE Trans. Electron Devices* **53**, 356–362 (2006).
7. Hu, Q. *et al.* Channel Engineering of Normally-OFF AlGaIn/GaN MOS-HEMTs by Atomic Layer Etching and High- κ Dielectric. *IEEE Electron Device Lett.* **39**, 1377–1380 (2018).
8. Efthymiou, L. *et al.* On the physical operation and optimization of the p-GaN gate in normally-off GaN HEMT devices. *Applied Physics Letters* **110**, 123502 (2017).
9. Meneghini, M. *et al.* Gate Stability of GaN-Based HEMTs with P-Type Gate. *Electronics* **5**, 14 (2016).
10. Liu, A.-C. *et al.* Improving Performance and Breakdown Voltage in Normally-Off GaN Recessed Gate MIS-HEMTs Using Atomic Layer Etching and Gate Field Plate for High-Power Device Applications. *Micromachines* **14**, 1582 (2023).



11. Zhang, T. *et al.* High-density 2D hole gas in p-GaN/AlN/AlGaN on a silicon substrate with polarization-enhanced Mg ionization. *Fundamental Research* S2667325823002182 (2023) doi:10.1016/j.fmre.2023.07.002.
12. Shao, P. *et al.* High density polarization-induced 2D hole gas enabled by elevating Al composition in GaN/AlGaN heterostructures. *Applied Physics Letters* **122**, 142102 (2023).
13. Ng, Y. H. *et al.* Distribution and transport of holes in the p-GaN/AlGaN/GaN heterostructure. *Applied Physics Letters* **123**, 142106 (2023).
14. Kumar, M. *et al.* p-GaN source integrated GaN/AlGaN/GaN double heterojunction field-effect transistor (FET) for next-generation electronic applications. *Sci Rep* **15**, 36710 (2025).
15. Thermal Annealing Effects on P-Type Mg-Doped GaN Films. *Jpn. J. Appl. Phys.* **31**, 139–142 (1992).
16. Kozodoy, P. *et al.* Heavy doping effects in Mg-doped GaN. *Journal of Applied Physics* **87**, 1832–1835 (2000).
17. Kumar, A. *et al.* Acceptor activation of Mg-doped GaN—Effects of N₂/O₂ vs N₂ as ambient gas during annealing. *Journal of Applied Physics* **134**, 035701 (2023).
18. Hull, B. A., Mohney, S. E., Venugopalan, H. S. & Ramer, J. C. Influence of oxygen on the activation of p-type GaN. *Applied Physics Letters* **76**, 2271–2273 (2000).
19. Kuo, C. H. *et al.* Low Temperature Activation of Mg-Doped GaN in O₂ Ambient. *Jpn. J. Appl. Phys.* **41**, L112–L114 (2002).
20. Garbe, V. *et al.* Ultra-low resistance Au-free V/Al/Ti/TiN ohmic contacts for AlGaN/GaN HEMTs. *Applied Physics Letters* **123**, 203506 (2023).
21. Wickenden, A. E., Koleske, D. D., Henry, R. L., Twigg, M. E. & Fatemi, M. Resistivity control in unintentionally doped GaN films grown by MOCVD. *Journal of Crystal Growth* **260**, 54–62 (2004).
22. Peta, K. R. *et al.* Analysis of electrical properties and deep level defects in undoped GaN Schottky barrier diode. *Thin Solid Films* **534**, 603–608 (2013).



23. Seager, C. H., Wright, A. F., Yu, J. & Götz, W. Role of carbon in GaN. *Journal of Applied Physics* **92**, 6553–6560 (2002). Article Online
DOI: 10.1039/D3TC04494D
24. Yang, J. *et al.* Investigation on the compensation effect of residual carbon impurities in low temperature grown Mg doped GaN films. *Journal of Applied Physics* **115**, 163704 (2014).
25. Qi, H. R. *et al.* Compensation of magnesium by residual carbon impurities in p-type GaN grown by MOCVD.
26. Koide, Y. *et al.* Effects of annealing in an oxygen ambient on electrical properties of ohmic contacts to p-type GaN. *Journal of Elec Materi* **28**, 341–346 (1999).
27. Götz, W., Johnson, N. M., Walker, J., Bour, D. P. & Street, R. A. Activation of acceptors in Mg-doped GaN grown by metalorganic chemical vapor deposition. *Applied Physics Letters* **68**, 667–669 (1996).
28. Brochen, S. *et al.* Dependence of the Mg-related acceptor ionization energy with the acceptor concentration in p-type GaN layers grown by molecular beam epitaxy. *Applied Physics Letters* **103**, 032102 (2013).
29. Nakajima, A. *et al.* Generation and transportation mechanisms for two-dimensional hole gases in GaN/AlGaIn/GaN double heterostructures. *Journal of Applied Physics* **115**, 153707 (2014).
30. Beckmann, C. *et al.* MOVPE-grown GaN/AlGaIn heterostructures on sapphire with polarization-induced two-dimensional hole gases. *J. Phys. D: Appl. Phys.* **55**, 435102 (2022).
31. Nakajima, A. *et al.* Temperature-Independent Two-Dimensional Hole Gas Confined at GaN/AlGaIn Heterointerface. *Appl. Phys. Express* **6**, 091002 (2013).
32. Bader, S. J. *et al.* Wurtzite phonons and the mobility of a GaN/AlN 2D hole gas. *Applied Physics Letters* **114**, 253501 (2019).
33. Poncé, S., Jena, D. & Giustino, F. Route to High Hole Mobility in GaN via Reversal of Crystal-Field Splitting. *Phys. Rev. Lett.* **123**, 096602 (2019).
34. Zhang, Z. *et al.* Polarization-induced 2D hole gases in pseudomorphic undoped GaN/AlN heterostructures on single-crystal AlN substrates. *Applied Physics Letters* **119**, 162104 (2021).



Open Access Article. Published on 14 April 2026. Downloaded on 4/15/2026 3:10:42 AM.
This article is licensed under a Creative Commons Attribution-NonCommercial 3.0 Unported Licence.



View Article Online
DOI: 10.1039/D5TC04494D

Data availability statement

The data supporting this article have been included as part of the Supplementary Information.

Open Access Article. Published on 14 April 2026. Downloaded on 4/15/2026 3:10:42 AM.
This article is licensed under a Creative Commons Attribution-NonCommercial 3.0 Unported Licence.

